Clinical Neurophysiology 122 (2011) 1429–1439

Contents lists available at ScienceDirect

Clinical Neurophysiology

journal homepage: www.elsevier.com/locate/clinph

Single-trial detection of somatosensory evoked potentials by probabilistic independent component analysis and wavelet filtering

L. Hu [a,c], Z.G. Zhang [b], Y.S. Hung [b], K.D.K. Luk [a], G.D. Iannetti [c], Y. Hu [a,*]

[a] Department of Orthopaedics and Traumatology, The University of Hong Kong, Hong Kong, China
[b] Department of Electrical and Electronic Engineering, The University of Hong Kong, Hong Kong, China
[c] Department of Neuroscience, Physiology and Pharmacology, University College London, UK

See Editorial, pages 1280–1281

ARTICLE INFO

Article history:
Available online 4 February 2011

Keywords:
Somatosensory evoked potentials (SEPs)
Event-related potentials (ERPs)
Single-trial analysis
Probabilistic independent component analysis (PICA)
Wavelet filtering

ABSTRACT

Objective: To develop an effective approach for enhancing the signal-to-noise ratio (SNR) and identifying single-trial short-latency somatosensory evoked potentials (SEPs) from multi-channel electroencephalography (EEG).
Methods: 128-channel SEPs elicited by electrical stimuli of the left posterior tibial nerve were recorded from 11 healthy subjects. Probabilistic independent component analysis (PICA) was used as a spatial filter to isolate SEP-related independent components (ICs), and wavelet filtering was used as a time–frequency filter to further enhance the SNR of single-trial SEPs.
Results: SEP-related ICs, identified using PICA, showed typical patterns of cortical SEP complex (P39–N50–P60) and scalp topography (centrally distributed with the spatial peak located near vertex). In addition, wavelet filtering significantly enhanced the SNR of single-trial SEPs ($p = 0.001$).
Conclusions: Combining PICA and wavelet filtering offers a space–time–frequency filter that can be used to enhance the SNR of single-trial SEPs greatly, thus providing a reliable estimation of single-trial SEPs.
Significance: This method can be used to detect single-trial SEPs and other types of evoked potentials (EPs) in various sensory modalities, thus facilitating the exploration of single-trial dynamics between EPs, behavioural variables (e.g., intensity of perception), as well as abnormalities in intraoperative neurophysiological monitoring.
© 2011 International Federation of Clinical Neurophysiology. Published by Elsevier Ireland Ltd. All rights reserved.

1. Introduction

Somatosensory evoked potentials (SEPs) are brain electrical responses following an applied somatosensory stimulus of a sensory or mixed sensorimotor peripheral nerve (Mauguiere et al., 1999; Nuwer et al., 1994). SEPs are commonly used to examine the functional integrity of somatosensory pathways, from the peripheral sensory nerves to the sensory areas of the brain (Blum and Rutkove, 2007). In clinical practice, SEPs have topodiagnostic values, and can be used to identify the existence of a lesion in the somatosensory pathways, to localize the lesion, thus providing a prognostic guide (Cruccu et al., 2008; Kraft et al., 1998). In operating theatres, SEPs can be used to monitor the function of somatosensory afferent pathways during surgery, thus preventing possible surgical injury (Cruccu et al., 2008; Deletis and Shils, 2002; Hu et al., 2001a).

As low-amplitude stimulus-evoked responses are embedded in relatively high amount of electrical noise caused by background ongoing EEG and other non-cortical artifacts, the SNR of SEPs is very low, and across-trial averaging in the time domain (Dawson, 1951, 1954) using at least 500 trials is recommended to identify and characterize short-latency SEPs (Cruccu et al., 2008). The obtained SEP waveform takes the form of a cortical complex (i.e., P39–N45–P60 for tibial-nerve SEPs, Cruccu et al., 2008; Mauguiere et al., 1999) relative to the onset of the sensory event. The basic assumption underlying this procedure is that evoked potentials (EPs) are stationary (i.e., their latency and morphology are invariant) and is therefore unaffected by the averaging procedure (Hu et al., 2010). In contrast, ongoing EEG activity behaves as noise

* Corresponding author. Address: Department of Orthopaedics and Traumatology, The University of Hong Kong, Duchess of Kent Children's Hospital, 12 Sandy Bay Road, Hong Kong, China. Tel.: +852 29740359; fax: +852 29740335.
E-mail address: yhud@hkusua.hku.hk (Y. Hu).

1388-2457/$36.00 © 2011 International Federation of Clinical Neurophysiology. Published by Elsevier Ireland Ltd. All rights reserved.
doi:10.1016/j.clinph.2010.12.052

unrelated to the event, and will therefore be largely cancelled out by averaging a large number of trials (Mouraux and Iannetti, 2008). However, SEPs are comprised of multiple waves (Cruccu et al., 2008; Mauguiere et al., 1999) whose latency and amplitude can independently vary from trial to trial (Spencer, 2005). Consequently, the across-trial averaging approach has the drawback that all the information concerning across-trial variability of SEPs is lost. Thus, across-trial averaging can heavily bias the representation of cortical activity elicited by a somatosensory stimulus, as across-trial variability often contains physiological information, for example, related to changes in stimulus parameters (duration, intensity, and rate) and fluctuations in surgical variables (blood pressure and temperature) (Mouraux and Iannetti, 2008; Wiedemayer et al., 2002). For this reason, the ability to obtain a reliable single-trial estimation of SEPs is highly desirable, as it would facilitate the exploration of single-trial dynamics between SEP measures, behavioural variables (e.g., intensity of perception, reaction time) (Iannetti et al., 2005), as well as abnormalities in intraoperative neurophysiological monitoring (e.g., SEPs in intraoperative spinal cord monitoring) (Hu et al., 2001b; Luk et al., 1999, 2001; Minahan, 2002; Nuwer, 1998).

The main challenge to obtain a reliable estimation of the single-trial SEP responses is how to enhance their SNR effectively and reliably. Several methods have been recently developed for accurately estimating the latency and amplitude of single-trial event-related potentials (ERPs). Second-order blind identification (SOBI) (Tang et al., 2005) and independent component analysis (ICA) (Jung et al., 2001) were adopted to detect the signal-trial ERPs, and the results showed that stimulus-related independent components (ICs) can be effectively separated from multi-channel EEG recordings, and SNR can be considerably increased in single trials. In addition, Mayhew et al. (2006) used a multiple linear regression method to estimate the latency and amplitude of laser evoked potentials (LEPs). Hu et al. (2010) further combined wavelet filtering and the multiple linear regression method to enhance the SNR, thus achieving robust single-trial estimate of even smaller ERP components (e.g., the N1 wave of LEPs). Britton et al. (2000) proposed to use the time sequence adaptive filtering and adaptive multi-resolution analysis for extracting single-trial ERPs. Mouraux and Plaghki (2004) employed a time–frequency analysis (TFA) using the wavelet transform to enhance SNR and disclose single-trial LEPs. Nishida et al. (1993) used three kinds of band-pass filters to detect the single SEP waveform, and Rossi et al. (2007) adopted an autoregressive filter with exogenous input on single-trial SEP extraction.

Among these methods, spatial–temporal filtering based on blind source separation (BSS) methods (e.g., ICA and SOBI) (Bingham and Hyvarinen, 2000; Hyvarinen, 1999; Hyvarinen and Oja, 2000; Jung et al., 2001; Makeig et al., 1997) has been demonstrated to be effective in isolating stimulus-related responses from multi-channel EEG recordings. In addition, time–frequency filtering (based on time–frequency decomposition methods such as windowed Fourier transform or wavelet transform) (Jongsma et al., 2006; Mouraux and Plaghki, 2004; Quiroga, 2000; Quiroga and Garcia, 2003) can be used to isolate stimulus-related, phase-locked responses from background EEG and non-cerebral artifacts. However, the combination of these two kinds of methods, which offers space–time–frequency filtering, has never been reported for single-trial SEP extraction.

This paper is the first attempt to develop a space–time–frequency filtering method that combines probabilistic ICA (PICA)-based spatial filtering with wavelet-based time–frequency filtering in order to enhance the SNR of SEPs in single trials. The PICA (Beckmann, 2004; Beckmann and Smith, 2004; Liang et al., 2010; Mouraux and Iannetti, 2009) method is used as a spatial filter to identify SEP-related ICs from multi-channel EEG recordings. As it is not convenient to record SEPs using 128 channels in both clinical applications and intraoperative monitoring, fewer-channel montages are more preferable. For this reason, the performances of SEPs at peak channel, which captures the highest SEP power, when using montages with fewer (64, 32, 16, and 8) channels have been evaluated to provide a recommended montage with quantitative evidence. Using the recommended montage, single-trial SEP detection can be achieved using the proposed method quickly and reliably. Furthermore, the peak channel was selected for subsequent time–frequency filtering based on continuous wavelet transform (CWT) (Mouraux and Plaghki, 2004; Tognola et al., 1998). The SNR of SEP responses before and after wavelet filtering is compared to illustrate the effectiveness of the proposed method. Finally, representative amplitudes from filtered SEP recordings and filtered resting EEG using the proposed method are compared to assess the validity of the space–time–frequency filtering method.

2. Methods

2.1. Data acquisition and preprocessing

Eleven young healthy volunteers (nine males and two females) participated in this study, with mean age of 27.4 ± 3.5 years (range 23–35 years). All participants gave written informed consent, and the local ethics committee approved the experimental procedures.

Subjects were seated in a quiet and comfortable room, and were instructed to relax, keep their eyes open and focus their attention on the stimuli. During the experimental sessions, repetitive electrical stimulation (1.1 Hz) was administered transcutaneously to the posterior tibial nerve (PTN), at the left ankle. The stimuli consisted in constant current square wave pulses (duration 0.1 ms), with intensity set just above the motor threshold, i.e., the intensity at which a clear muscle twitch in the abductor hallucis was observed. The average stimulus intensity was 21 ± 2 mA (range 18–25 mA). For each subject, about 330 stimuli, which lasted for 5 min in total, were delivered.

SEPs were recorded by a 128-channel NeuroScan System (pass band: 0.05–200 Hz, sampling rate: 1000 Hz), using a standard EEG cap based on the extended International 10–20 system, using Cz as reference channel. Channel impedances were kept lower than 10 kΩ. The locations of EEG channels were recorded with a 3D digitizer (Polhemus, Colchester, VT, USA). To monitor ocular movements and eye blinks, electro-oculographic (EOG) signals were simultaneously recorded from two surface channels, one placed over the lower eyelid, the other placed 1 cm lateral to the outer corner of the orbit. Continuous EEG data were band-pass filtered between 1 and 100 Hz. SEP trials were extracted using a window analysis time of 300 ms (100 ms pre-stimulus and 200 ms post-stimulus) and baseline corrected using the pre-stimulus time interval. Trials with large eye movements and muscle artefacts (exceeding 100 μV) were rejected automatically. After baseline correction and artefact rejection, 326 ± 3 trials were used for further SEP single-trial detection, and these SEP data were re-referenced to a common average reference.

2.2. Data processing

The procedures for single-trial detection of SEPs were summarized in Fig. 1, consisting of two consecutive steps: PICA-based spatial filtering and wavelet-based time–frequency filtering.

2.2.1. Probabilistic independent component analysis (PICA)

PICA was performed to separate EEG data into spatially-fixed and temporally-independent non-Gaussian sources and an additive Gaussian noise, which is actually a combination of probabilis-

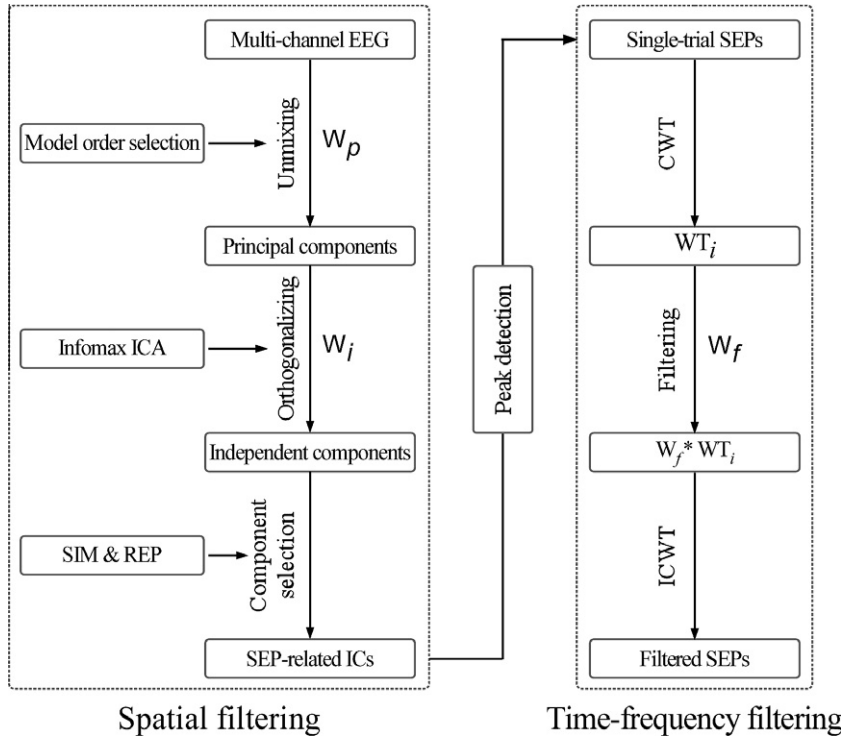

Fig. 1. Flowchart describing single-trial detection of short-latency SEPs. *Left panel*: spatial filtering combined PPCA and Infomax ICA into PICA, and then used a joint SIM and REP criteria to isolate and separate SEP-related ICs. *Right panel*: time–frequency filtering based on CWT was imposed on single-trial SEPs at peak channel to further enhance their SNR.

tic principal component analysis (PPCA) (Beckmann and Smith, 2004; Minka, 2001; Tipping and Bishop, 1999a,b) and an information maximization algorithm (Infomax ICA) (Bell and Sejnowski, 1995; Delorme and Makeig, 2004). In theory, PPCA was used to decompose an EEG signal into a specified number of principal components (PCs) and a Gaussian noise residual. The subspace of the PCs was then orthogonalized by Infomax ICA (Bell and Sejnowski, 1995) to obtain the temporally-independent ICs.

Firstly, PPCA decomposed the EEG data into a lower dimensional source subspace and a noise subspace using maximum-likelihood density estimation (Tipping and Bishop, 1999b). The PPCA model can be characterized by defining a high-dimensional vector of observations as a linear combination of low-dimensional PCs plus an additive Gaussian noise:

$$\mathbf{x} = \mathbf{A}\mathbf{y} + \boldsymbol{\mu} + \mathbf{n} \tag{1}$$

where $\mathbf{x}$ represents a d-dimensional vector of multi-channel EEG data, $\mathbf{y}$ denotes a k-dimensional ($k \leqslant d$) vector of PCs with distribution $\mathbf{y} \sim \mathcal{N}(\mathbf{0}, \mathbf{I_k})$, $\boldsymbol{\mu}$ is the mean of $\mathbf{x}$, $\mathbf{A}$ denotes the mixing matrix, and $\mathbf{n}$ is Gaussian noise with distribution $\mathbf{n} \sim \mathcal{N}(0, \sigma^2\mathbf{I}_d)$. The inverse of the mixing matrix $\mathbf{A}$ gives the unmixing matrix $\mathbf{W}_p$, which will be used for validity test, as described in Section 2.2.4. With this model, the distribution of observed data $\mathbf{x}$ is:

$$\mathbf{x} \sim \mathcal{N}(\boldsymbol{\mu}, \mathbf{A}\mathbf{A}^T + \sigma^2\mathbf{I}_d) \tag{2}$$

Based on the maximum-likelihood density estimation (Minka, 2001; Tipping and Bishop, 1999a,b), we have

$$\boldsymbol{\mu}_{ML} = \frac{1}{N}\sum_{i=1}^{N}\mathbf{x}_i \tag{3}$$

$$\mathbf{S} = \frac{1}{N}\sum_{i=1}^{N}(\mathbf{x}_i - \boldsymbol{\mu})(\mathbf{x}_i - \boldsymbol{\mu})^T \tag{4}$$

$$\mathbf{A}_{ML} = \mathbf{U}_k(\boldsymbol{\Lambda}_k - \sigma^2\mathbf{I}_k)^{1/2}\mathbf{R} \tag{5}$$

$$\sigma^2_{ML} = \frac{1}{d-k}\sum_{j=k+1}^{d}\lambda_j \tag{6}$$

where the column orthogonal matrix $\mathbf{U}_k$ contains the top k eigenvectors of $\mathbf{S}$, $\boldsymbol{\Lambda}_k$ is the diagonal matrix containing the top k eigenvalues of $\mathbf{S}$, λ_j is the (j,j)th entry of $\boldsymbol{\Lambda}_k$, and $\mathbf{R}$ is an orthogonal matrix, which is generally taken as $\mathbf{R} = \mathbf{I}$. A more complicated expectation-maximization (EM) algorithm (Roweis, 1998) can also be used for an efficient calculation of $\mathbf{R}$.

Here, the number of sources that determine the valid subspace should be accurately estimated prior to the PC estimation. An effective method, initially developed by Beckmann and Smith (2004) for the analysis of fMRI data and also used by Mouraux and Iannetti (2009) and Liang et al. (2010) in EEG studies, is adopted in this study to estimate the number of sources and to identify/isolate SEP-related ICs contained in the multi-channel EEG. The basic idea underlying this method is to combine a Laplace approximation with the predicted cumulative distribution, and to adjust the eigenspectrum (to give an adjusted Laplace approximation) (Beckmann and Smith, 2004). For more details, please refer to Beckmann and Smith (2004).

Once PCs have been identified by PPCA, multidimensional orthogonal vectors were transformed into ICs with maximal statistical independence from each other. In this study, the orthogonal procedure was performed on the obtained PCs using Infomax ICA (Bell and Sejnowski, 1995; Delorme and Makeig, 2004). Consequently, ICs (with the same dimension as the PCs) and the corresponding orthogonalizing matrix $\mathbf{W}_i$ were obtained for each subject.

To identify SEP-related ICs from all the obtained ICs (i.e., to distinguish SEP-related ICs from noise-related ICs), two measures,

namely the similarity index (SIM) and the relative power (REP), were used to classify ICs. The SIM estimates the similarity of responses between single trials and their average, while the REP estimates the power increase after the presentation of the stimuli compared to the pre-stimulus interval on the averaged waveform.

The SIM of each IC within the post-stimulus interval (0–100 ms) is calculated as

$$\hat{\mathrm{SIM}} = \frac{\hat{\sigma}_X^2 - \hat{\sigma}_N^2}{\hat{\sigma}_X^2} \tag{7}$$

$$\hat{\sigma}_X^2 = \frac{\sum_j \sum_t x_j^2(t)}{T(J-1)} \tag{8}$$

$$\hat{\sigma}_N^2 = \frac{\sum_j \sum_t [x_j(t) - \bar{x}(t)]^2}{T(J-1)} \tag{9}$$

where $\hat{\sigma}_X^2$ is the power of ICs and $\hat{\sigma}_N^2$ is the power of noise (estimated as $x_j - \bar{x}$), $x_j(t)$ is the single-trial waveform of a SEP-related IC ($j = 1, \ldots, J$ is the trial number and $t = 1, \ldots, T$ is the time point after stimulus), and $\bar{x}$ is the average across all single trials (Tang et al., 2005). SEP-related ICs often possess a higher SIM than non-stimulus-locked ICs and noise-related ICs.

The REP is obtained as the ratio between the mean post-stimulus power and the mean pre-stimulus power on the averaged SEPs for each subject (Mouraux and Iannetti, 2009). SEP-related ICs, which correspond to the stimulus-evoked responses, often capture an increase of power after the sensory stimulus. Thus, SEP-related ICs have higher REP values than noise-related ICs.

A joint criteria of both SIM ($\mathrm{SIM} > 70\% \times (\max(\mathrm{SIM}) - \min(\mathrm{SIM})) + \min(\mathrm{SIM})$) and REP ($\mathrm{REP} > 4$) were adopted in this study. The ICs satisfying both criteria were classified as SEP-related ICs, while others were classified as noise-related ICs. It is necessary to highlight that the obtained classification was not critically dependent on the arbitrary selected threshold of SIM = 70% and REP = 4. Indeed, lower threshold values, like SIM = 50% and REP = 2, would recruit several small-weighted ICs (i.e., those that explained a small portion of the total variance of the data), but they would not result in much difference of SEP responses at peak channel from those obtained using more stringent threshold values.

Waveform shapes, peak topographies and dipole sources, i.e., the response features typically used to recognize ICs (Britton et al., 2000; Tang et al., 2005), were used to verify the accuracy of the proposed criteria (Fig. 2). Here, the source locations of SEP-related ICs were modeled by fitting a single equivalent dipole or two symmetrical equivalent dipoles for each IC. Dipole fitting was performed using dipfit2 algorithm with a standardized boundary element head model in EEGLAB (Delorme and Makeig, 2004). Dipole locations outside the head, and dipole models with a residual variance (RV) exceeding 20% were excluded.

The optimal number of dipoles was determined by the following procedures.

(1) To calculate the RV for both models (a single dipole model and two symmetrical dipoles model), each SEP-related IC was modeled by fitting a single dipole and by fitting two symmetrical equivalent dipoles consecutively.

As we known, the model with more parameters (two symmetrical dipoles) would always fit the data at least as well as the model with fewer parameters (a single dipole). Therefore, the complicate model would give a better fit to the data (the scalp distribution of each IC) than the simple model. However, the model with more parameters would fit more noise than that of the model with fewer parameters (i.e., over-fitting).

(2) To select the optimal dipole model and to avoid possible problems of under-fitting or over-fitting, the Bayesian information criterion (BIC, or Schwarz criterion) (Schwarz, 1978) was adopted. This BIC criterion was proved to be able to provide a more accurate estimation of the number of dipole sources for the 128-channel montage regardless of the noise level than several other model estimation approaches (e.g., Akaike's criterion and Hannan-Quinn information criterion) (Bai and He, 2005, 2006), and it can be expressed as

$$\mathrm{BIC}_n = m \log(E_n^2) + \mathrm{DF}_n \log(m) \tag{10}$$

where BIC is the estimated Bayesian information criterion value, n is the number of dipoles (1 or 2 in this study), m is the number of channels, $\log(\bullet)$ is the natural logarithm, E_n^2 is the error function (RV in this study), and DF is the number of parameters for describing n dipoles (six for a single dipole and nine for two symmetrical dipoles). The dipole model with minimum BIC_n is supported as the optimal model, and n is the optimal dipole number, which was used for further dipole fitting analysis.

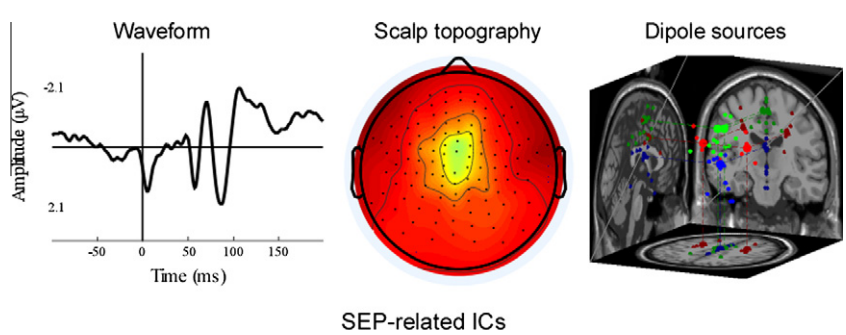

Fig. 2. Waveform, scalp topography and dipole sources of SEP-related ICs. *Left panel*: representative waveform of SEP-related ICs showing a typical "W" shape between 30 and 120 ms following the presentation of electrical stimuli. Note that the positive deflection appearing at about 5 ms after the onset of the stimulus is the artifact generated by electrical stimulation. *Middle panel*: representative scalp topography of SEP-related ICs which is centrally distributed with the peak located near vertex. Note that similar scalp topographies were obtained from all subjects. *Right panel*: source locations of SEP-related ICs were modeled by fitting a single dipole or two symmetrical equivalent dipoles for each SEP-related IC. The locations of the fitted dipoles were classified to form three clusters: a bilateral cluster was located in the left and right operculo-insular regions (x =±26 mm, y = 0.4 mm, z = 36 mm). While, the deep midline cluster (existing in 6 of 11 subjects) was located in cingulate cortex (x =±0.2 mm, y = −10 mm, z = 18 mm), the superficial midline cluster (existing in 10 of 11 subjects) was mainly located in the primary somatosensory cortex (x =±3.2 mm, y = −10 mm, z = 55 mm). The smaller spheres represented the dipole locations of each single SEP-related IC, and the larger sphere showed the center of gravity of each cluster (bilateral cluster, deep midline cluster, and superficial midline cluster are shown in red, blue, and green, respectively). (For interpretation of the references in colour in this figure legend, the reader is referred to the web version of this article.)

After the removal of noise-related ICs, the channel displaying the largest SEP responses was identified based on the post-stimulus power. The single-trial responses at this channel (hereinafter referred to as the peak channel) were selected for further time–frequency filtering. The peak channel (represented as one channel) was selected because the short-latency SEPs were believed to be generated from primary somatosensory cortex (SI) in the postcentral gyrus (both Brodmann areas 3b and 1) (Baumgartner et al., 1998; Cruccu et al., 2008). Similarly, van de Wassenberg et al. (2008a,b) showed that the scalp topographies of typical short-latency SEPs are similar with each other (N20–P27–P45 for median nerve SEPs [Fig. 2 in their publication], P39–N50–P60 for tibial-nerve SEPs [Fig. 1 in their publication]). Indeed, different channels should be used when measuring both short-latency and long-latency SEP responses, because the short-latency and long-latency SEP responses were generated from spatially distinct sources (their distance is much larger than that between Brodmann areas 3b and 1).

In order to show the filter effect of spatial filtering using PICA, we estimated the SNR of single-trial SEPs (both single channel and the mean across all channels) before and after spatial filtering as (Tang et al., 2005):

$$\hat{\mathrm{SNR}} = \frac{\hat{\sigma}_X^2 - \hat{\sigma}_N^2}{\hat{\sigma}_N^2} \tag{11}$$

where $\hat{\sigma}_X^2$ is the power of single-trial SEP waveform and $\hat{\sigma}_N^2$ is the power of noise (estimated as the difference between single-trial SEP waveform and the average across all trials). The SNRs before and after spatial filtering were compared using two tailed Wilcoxon Signed Ranks test.

2.2.2. Performance of fewer-channel montages

After PICA, the SNR and power of spatial filtered SEP responses (at the peak channel and averaged across all channels) in the post-stimulus interval were calculated from 64, 32, 16, and 8-channel montages (according to the International 10–20 system), and they were further compared with the SNR and power values calculated for the original 128-channel montage. To test the differences between these montages, the non-parametric Friedman's ANOVA was used, as the SNR and power values were not normally distributed (Debener et al., 2007; Hu et al., 2010; Spencer, 2005). When differences were significant, we performed a post hoc analysis using the Wilcoxon Signed Ranks test.

2.2.3. Time–frequency filtering

The continuous wavelet transform (CWT) based time–frequency filtering was performed by means of the following three steps. First, single-trial SEP waveforms were decomposed into a time–frequency representation using CWT. Second, specific areas on the time–frequency plane corresponding to the SEP responses were identified and used to generate the wavelet filtering model. Third, time-domain SEP waveforms were reconstructed from the filtered time–frequency representation using inverse CWT (ICWT).

The time–frequency representation of each single SEP trial was calculated using the CWT, which is defined as (Tognola et al., 1998):

$$\mathrm{WT}(\tau,f) = \int_t x(t) \cdot \sqrt{f/f_0} \cdot \psi^*(f/f_0 \cdot (t-\tau))dt \tag{12}$$

$$\psi(t) = \frac{1}{\sqrt{\pi f_b}} e^{2\pi i f_0 t} e^{-t^2/f_b} \tag{13}$$

where τ and f are the time and frequency index, respectively; $x(t)$ is the original signal in the time (t) domain; $\psi(t)$ is the mother wavelet function with center frequency f_0 and bandwidth f_b. The mother wavelet $\psi(t)$ used in this paper is a complex Morlet wavelet (Eq. 13). The bandwidth parameter f_b was set to 0.05, and the wavelet center frequency f_0 was set to 6. The squared magnitude of $WT(\tau,f)$, called the scalogram, showed a good time–frequency resolution with explored frequencies ranging from 1 to 100 Hz in steps of 1 Hz.

For each estimated frequency, the magnitude of the power spectrum was baseline-corrected (i.e., normalized) by subtracting the average power of the signal enclosed in the time-interval between −50 and 0 ms (Iannetti et al., 2008; Pfurtscheller and Lopes da Silva, 1999). The group level time–frequency representation WT_{total} was obtained by averaging the normalized WT from all subjects. The obtained time–frequency matrix was then thresholded with the objective of keeping wavelet coefficients with high power and eliminating wavelet coefficients with low power. In order to apply time–frequency filtering to enhance the SNR of the short-latency SEPs at single-trial level, a binary time–frequency template (W_f) was generated. The template W_f was obtained by creating a matrix whose time–frequency pixels were set to 1 when the power of the corresponding wavelet coefficient was greater than the threshold, and set to 0 when the power was smaller than the threshold. The threshold parameter is defined as $0.9*(P_{\max} - P_{\min}) + P_{\min}$ where $P_{\max}$ is the maximum power of the wavelet coefficients and $P_{\min}$ is the minimum power. The time–frequency template identifies the distribution of EEG changes induced by the somatosensory stimulus in the time–frequency domain, and is used to filter out the contribution of non-stimulus-related background.

For each single trial SEPs, time–frequency filtering was achieved by multiplying the time frequency representation of the single trial i, WT_i, with the binary weighting matrix W_f as

$$FWT_i(\tau,f) = W_f \cdot WT_i(\tau,f) \tag{14}$$

where FWT_i is the filtered time frequency representation.

The filtered single-trial signal $y_i(t)$ was finally reconstructed in the time domain from $FWT_i(\tau,f)$, using ICWT (Tognola et al., 1998):

$$y_i(t) = C_\psi \int_\tau \int_f FWT_i(\tau,f) \cdot \sqrt{f/f_0} \cdot \psi(f/f_0(t-\tau)) \cdot (f/f_0)^2 \cdot d\tau \cdot df \tag{15}$$

where $C_\psi = \int_0^\infty [|\Psi(f)|^2/f]df$ is a constant that depends on $\Psi(f)$, the Fourier transform of $\psi(t)$.

To evaluate the effect of the described wavelet filtering, we calculated the SNR of single-trial SEPs before and after time–frequency filtering using Eq. (11). The obtained SNRs before and after wavelet filtering were compared using two tailed Wilcoxon Signed Ranks test.

2.2.4. Validity test using ongoing EEG

In order to test whether the described method introduces any bias (i.e., the spurious result of aligning and filtering of ongoing EEG oscillations (Quiroga and Garcia, 2003)) in the analysis, we performed the same procedures on resting EEG signals, which were recorded from all subjects for this validation. For each subject, the unmixing matrix $\mathbf{W}_p$, the orthogonalizing matrix $\mathbf{W}_i$ from PICA and the time–frequency model $\mathbf{W}_f$ from the wavelet filtering (Fig. 1), which were all calculated from the SEP data, were applied to 100 trials of resting EEG. The performance of the described method on these 100 trials of resting EEG was compared with its performance on 100 SEP trials (the first 100 trials). The amplitude values obtained from the analysis of the resting EEG data were compared against zero using a one sample t test.

3. Results

3.1. SEP-related ICs

When applied to the 128-channel SEP recordings, a number of spatially-fixed and temporally-independent ICs were identified using PICA. These ICs were likely to represent both physiologically-independent neural activities and non-neural activities. The estimated number of ICs was, across subjects, 32 ± 13 (range 14–54) and accounted for 98.2 ± 1.3% of the total variance of the SEP data. The number of SEP-related ICs, identified by the joint SIM and REP criteria, was 2 ± 1 (range 1–5) across subjects. These SEP-related ICs contributed to 62.1 ± 22.6% of the variance of the averaged SEP responses.

These identified SEP-related ICs were often characterized with: (1) a regular shape in the post-stimulus interval (30–120 ms) of the across-trial averaged waveform (Fig. 2, *left panel*); (2) a centrally distributed scalp topography with the peak located near vertex channel (Cz) (Fig. 2, *middle panel*).

Based on the BIC criterion, the single dipole model was adopted for 6 (out of 25 in total) SEP-related ICs, and the two symmetrical dipoles model was adopted for 19 (out of 25 in total) SEP-related ICs. For each subject, 2.4 ± 1.4 SEP-related ICs were successfully modeled (residual variance: 5.4 ± 4.9%). The obtained dipoles were further classified into three clusters as follows (Fig. 2, *right panel*):

(1) Dipoles, of which the absolute x values were larger than 20 mm, were classified as a bilateral cluster ($x < -20$ mm or $x > 20$ mm, Montreal Neurological Institute coordinates).
(2) Dipoles, of which the absolute x values were less than 20 mm and the z-axis values were less than 30 mm, were

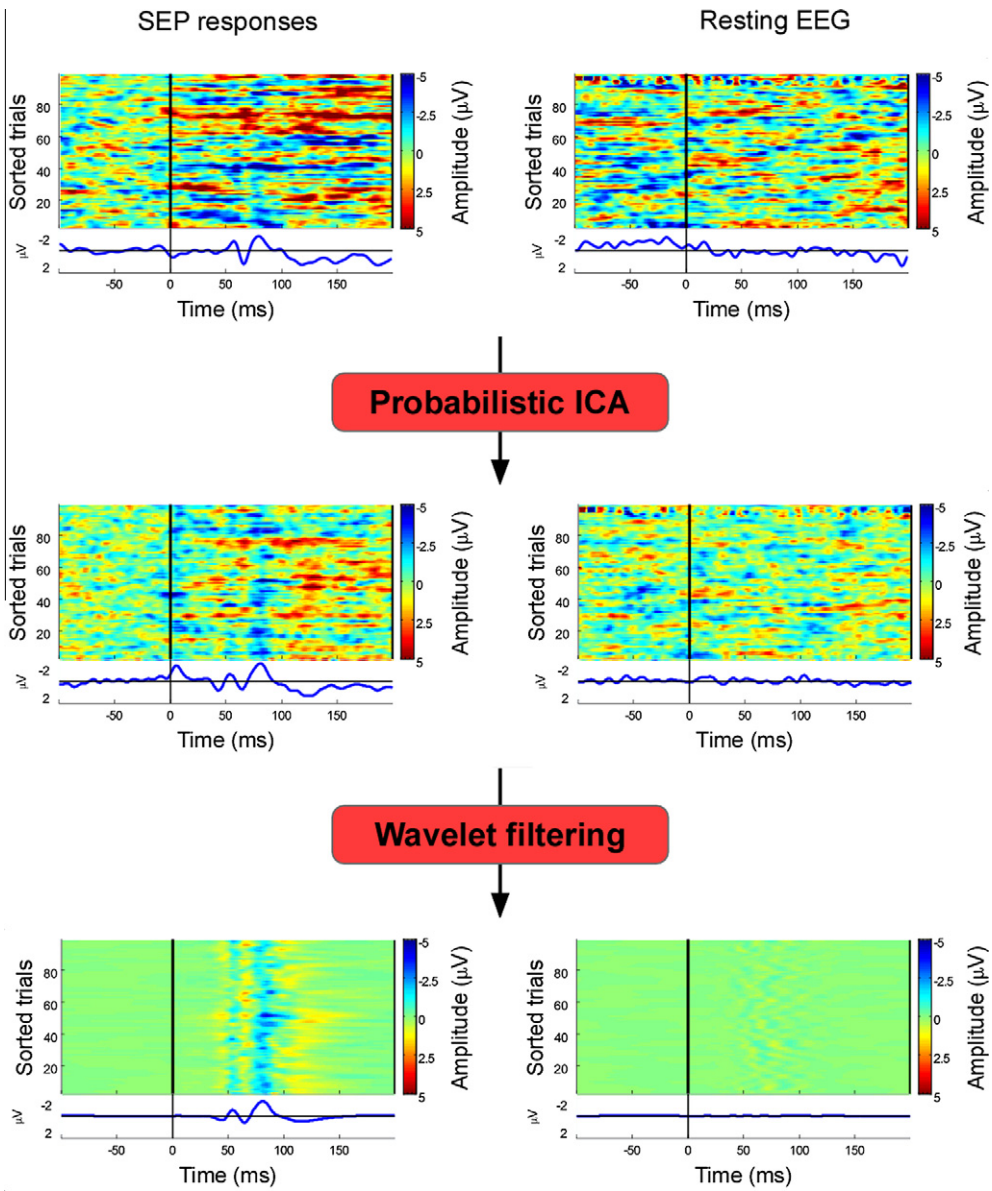

Fig. 3. The effect of space–time–frequency filtering on single-trial SEPs and resting EEG. *Top panel*: single-trial SEP responses and resting EEG were shown in the *left* and *right* of *top panel*, respectively (smoothing = 3). *Middle panel*: single-trial SEP responses and resting EEG, which have been spatially filtered, were shown in the *left* and *right* of *middle panel*, respectively. Note that the variation of single-trial resting EEG was markedly reduced, while single-trial SEP responses were more clearly presented. *Bottom panel*: single-trial SEP responses and resting EEG, which have been further time–frequency filtered, were displayed in the *left* and *right* of *bottom panel*, respectively. Results indicated that phase-locked responses of short latency SEPs were preserved with remarkably high SNR while resting EEG was almost identical to zero across all points along the time course.

classified as a deep midline cluster (-20 mm < x < 20 mm and z < 30 mm).

(3) Dipoles, of which the absolute x values were less than 20 mm and the z-axis values were larger than 30 mm, were classified as a superficial midline cluster (-20 mm < x < 20 mm and z > 30 mm).

The dipole locations in each cluster were averaged for the left and right hemispheres, respectively (Fig. 2, *right panel*). The bilateral cluster (existing in 3 of 11 subjects) was located in the left and right operculo-insular regions (x =±26 mm, y = 0.4 mm, z = 36 mm). While, the deep midline cluster (existing in 6 of 11 subjects) was located in cingulate cortex (x =±0.2 mm, y = -10 mm, z = 18 mm), the superficial midline cluster (existing in 10 of 11 subjects) was mainly located in the primary somatosensory cortex (x =±3.2 mm, y = -10 mm, z = 55 mm).

After removing noise-related ICs based on the joint SIM and REP criteria, single-trial SEP responses at the peak channel were more clearly presented (Fig. 3, *top* and *middle panels*).

When evaluating on the peak channel, spatial filtering enhanced (but not significantly) the SNR of single-trial SEP responses (SNR before spatial filtering: 0.031 ± 0.023; after spatial filtering: 0.046 ± 0.027, 1.86 ± 1.33 times enhanced, p = 0.062, two tailed Wilcoxon Signed Ranks test). When evaluating on all channels; spatial filtering significantly enhanced the SNR of single-trial SEP responses (SNR before spatial filtering: 0.005 ± 0.002; after spatial filtering: 0.023 ± 0.017, 5.41 ± 4.04 times enhanced, p = 0.008, two tailed Wilcoxon Signed Ranks test).

The difference (between the significant improvement of the estimated SNR when considering all channels and the less improvement when considering only the peak channel) may be caused by the reason that spatial filtering using PICA is able to identify and remove some noise (e.g., artifacts related to the activity of *temoralis* muscle and artifacts related to eye blink and movement), which may or may not contaminate the signal recorded at the peak channel (near Cz). If these artifacts were small in magnitude and did not affect the peak-channel signal, the removal of these noise-related ICs could not improve the SNR at the peak channel significantly, but can improve the SNR across all channels. If these artifacts were large in magnitude and affected the peak-channel signal greatly, the removal of these noise-related ICs could help improve the SNR of both single channel and all channels.

3.2. Performance of fewer-channel montages

Similarly, when considering the peak channel, PICA cannot significantly improve the SNR in most cases (64-channel: p = 0.003; 32-channel: p = 0.965; 16-channel: p = 0.541; 8-channel: p = 0.657). However, when considering all recording channels, PICA significantly improved the SNR for all montages (64-channel: p = 0.013; 32-channel: p = 0.003; 16-channel: p = 0.003; 8-channel: p = 0.003).

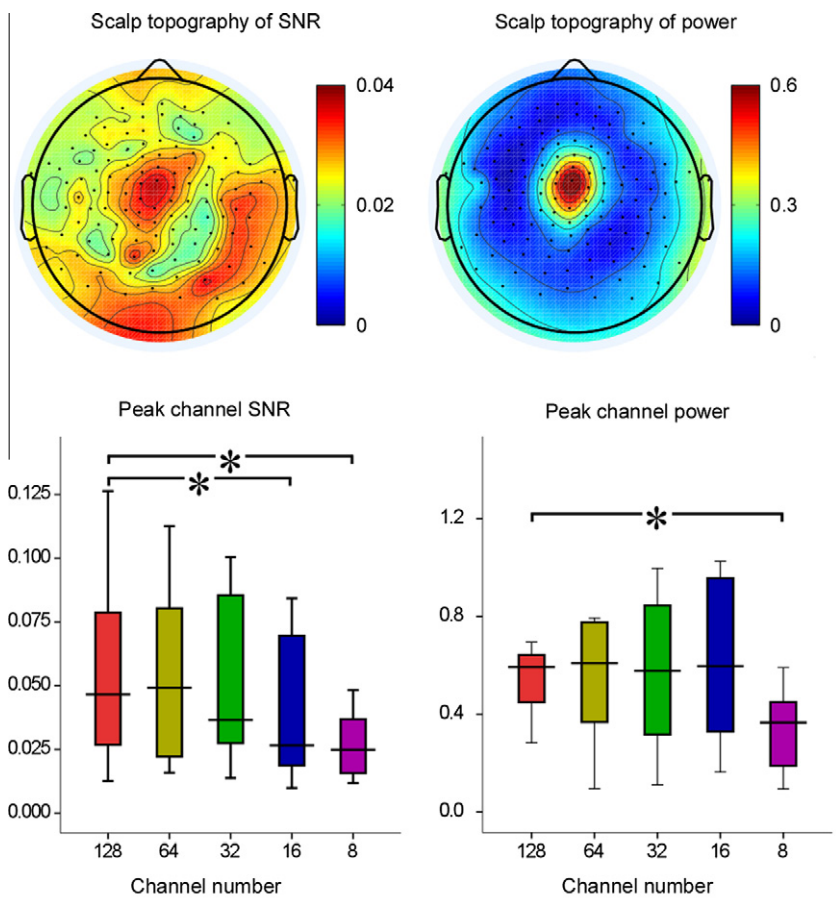

Fig. 4. Group average scalp topographies of SNR and power, and peak channel SNR and power measured from different montages. *Top left panel*: the group-average scalp topography of SNR, which displayed a higher SNR distribution around central region (Cz) and contralateral temporal region (T4). *Top right panel*: the group-average scalp topography of power, which displayed a very clear central distribution of the power (maximal around Cz). *Bottom left panel*: peak channel SNR measured from 128, 64, 32, 16, and 8-channel montages were compared across subjects. *Bottom right panel*: peak channel power measured from 128, 64, 32, 16, and 8-channel montages were compared across subjects. Horizontal black lines show the median values, while down and up borderline lines of the color box indicate the lower quartile, and upper quartile values. Asterisk * indicates a significant difference between values obtained from 128-channel and those from fewer channel montages. (For interpretation of the references in colour in this figure legend, the reader is referred to the web version of this article.)

Table 1
SNR measured at peak channel when using 128, 64, 32, 16, and 8-channel montages across all subjects.

Subjects	128-channel	64-channel	32-channel	16-channel	8-channel
#1	0.0243	0.0252	0.0252	0.0248	0.0249
#2	0.0126	0.0159	0.0141	0.0104	0.0123
#3	0.0294	0.0364	0.0343	0.0196	0.0182
#4	0.0466	0.0523	0.0436	0.0266	0.0276
#5	0.0437	0.0192	0.0297	0.0099	0.0133
#6	0.1263	0.0901	0.0972	0.0842	0.085
#7	0.0236	0.0171	0.0138	0.0179	0.0118
#8	0.0465	0.0491	0.0366	0.0446	0.0232
#9	0.0671	0.0773	0.1001	0.0841	0.0369
#10	0.0902	0.0833	0.0736	0.0593	0.0482
#11	0.1045	0.1126	0.1004	0.0798	0.0369
Median	0.0465	0.0491	0.0366	0.0266	0.0249
Lower quartile	0.02685	0.0222	0.02745	0.01875	0.01575
Upper quartile	0.07865	0.0803	0.0854	0.06955	0.0369

Table 2
Power measured at peak channel when using 128, 64, 32, 16, and 8-channel montages across all subjects.

Subjects	128-channel	64-channel	32-channel	16-channel	8-channel
#1	0.6091	0.7086	0.6275	0.7402	0.5907
#2	0.1335	0.0962	0.133	0.241	0.1842
#3	0.4016	0.5512	0.4771	0.3257	0.1905
#4	0.6744	0.6079	0.5772	0.4142	0.442
#5	0.4983	0.1841	0.2354	0.3327	0.3681
#6	2.6644	2.0707	2.7855	3.4721	2.2792
#7	0.2844	0.1856	0.112	0.1641	0.0947
#8	0.5477	0.6031	0.4001	0.5968	0.2838
#9	0.5922	0.7848	0.9963	1.0206	0.3665
#10	0.5984	0.7933	0.8343	0.8917	0.1884
#11	0.6948	0.7671	0.8544	1.0257	0.4583
Median	0.5922	0.6079	0.5772	0.5968	0.3665
Lower quartile	0.44995	0.3684	0.31775	0.3292	0.18945
Upper quartile	0.64175	0.77595	0.84435	0.95615	0.45015

The top left graph in Fig. 4 showed the group-average scalp topography of SNR, which displayed a higher SNR distribution around the central region (Cz) and the contralateral temporal region (T4). The top right graph in Fig. 4 showed the group average scalp topography of power, which displayed a very clear central distribution of the power (maximal around Cz). Both scalp topographies of the SNR and power indicated that short-latency SEPs were mainly generated from the SI.

There was a significant difference in peak channel SNR among 128, 64, 32, 16, 8-channel montages using Friedman's ANOVA ($\chi^2(2) = 22.16, p < 0.001$) (Fig. 4, bottom left panel, and Table 1). Post hoc comparisons between the peak channel SNR using the Wilcoxon Signed Ranks test revealed that there existed significant differences between 128-channel and 16-channel montages ($p = 0.019$), and between 128-channel and 8-channel montages ($p = 0.003$). Also, there was a significant difference in peak channel power among 128, 64, 32, 16, 8-channel montages ($\chi^2(2) = 10.98, p < 0.022$) (Fig. 4 bottom right panel, Table 2). Post hoc analysis using the Wilcoxon Signed Ranks test revealed a significant difference between the peak channel power of 128-channel and 8-channel montages ($p = 0.003$). These results showed that the peak channel SNR did not have significant difference when using 128, 64, and 32-channel montages, and the peak channel power did not have significant difference when using 128, 64, 32 and 16-channel montages.

3.3. Time–frequency filtering

The SNR of single-trial short-latency SEPs was increased using a time–frequency filter based on CWT. The left panel of Fig. 5 showed the averaged time–frequency representation of single-trial SEP responses from all subjects (top and bottom plots were, respectively, the time–frequency representations without and with baseline correction, which was achieved by subtracting the average power of the signal enclosed in the time-interval ranging between −50 and 0 ms). The baseline-corrected time–frequency representation, which was used to derive the wavelet filter model, was characterized by a phase-locked signal power increase between 30 and 120 ms in time, and between 30 and 60 Hz in frequency (Fig. 5, *left panel*). The bottom panel of Fig. 3 and the middle panel of Fig. 5 showed how this time–frequency filter reduced minimally the amplitude of the response and increased remarkably its SNR. In addition, the bottom panel of Fig. 3 showed the effect of the time–frequency filter on single-trial resting EEG. While in the SEP waveforms the wavelet filtering significantly enhanced the SNR of the phase-locked SEP responses (SNR before time–frequency filtering: 0.046 ± 0.027; after time–frequency filtering: 0.14 ± 0.11; 2.98 ± 1.29 times enhanced, $p = 0.001$, two tailed Wilcoxon Signed Ranks test) (Fig. 5, *right panel*), in the resting EEG the wavelet filtering only reduced the noise.

3.4. Validity test using ongoing EEG

To test if the space–time–frequency filtering method introduced any bias in the analysis, the same PICA and WT techniques were applied to 100 resting EEG trials obtained for each subject (Fig. 3).

Peak latencies of cortical SEP complex (P39–N50–P60) were measured from the averaged SEP waveforms for each subject, and the corresponding single-trial amplitudes at these latencies were measured from both filtered SEP recordings and filtered resting EEG. The single-trial amplitudes from resting EEG trials yielded a mean (±SD) amplitude value of −0.045 ± 0.37 μV, 0.025 ± 0.54 μV, and −0.026 ± 0.55 μV for P39, N50, and P60, respectively. These amplitude values were not significantly different from zero ($F = 1.429$, $p = 0.221$, one-way ANOVA). In contrast, the single-trial amplitude values from SEP trials yielded a mean (±SD) amplitude value of 1.39 ± 1.23 μV, −2.56 ± 2.17 μV, and 0.95 ± 1.96 μV for P39, N50, and P60, respectively. A comparison of the single-trial amplitudes obtained from the SEP waveforms and the resting EEG trials for a representative subject was shown in Fig. 6. This result confirmed that the described method provided an unbiased estimate of single-trial SEP responses without introducing any spurious result.

4. Discussion

In this study, a space–time–frequency filtering method which combined PICA-based spatial filtering and CWT-based time–frequency filtering was developed and applied to multi-channel SEP recordings. Three main findings were observed from the experimental results. First, we show that SEP-related activities can be successfully isolated by PICA with correct patterns of waveform shapes, peak topographies and dipole source locations. Second, we provide quantitative evidences, including peak channel SNR and peak channel power of SEP responses, to illustrate that a 32-channel montage is able to provide a reliable and accurate estimation of single-trial SEPs using the proposed method. Third, we show that, after removing noise by PICA, the SNR of SEP responses can be significantly enhanced using time–frequency filtering, both in average and single trials.

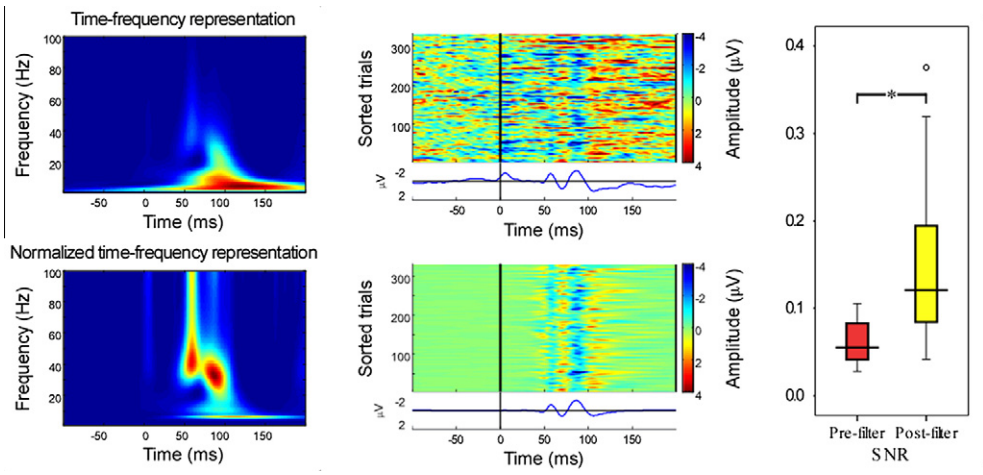

Fig. 5. Effect of time–frequency filtering on single-trial SEP responses. *Left panel*: time–frequency representation of SEP responses, obtained from CWT, is shown in the *top* of *Left panel*, while baseline corrected time–frequency representation which highlights phase-locked SEP responses is presented in the *bottom* of *left panel*. *Middle panel*: single-trial SEP responses and the time–frequency filtered responses are shown in the *top* and *bottom* of *middle panel* (smoothing = 3). *Right panel*: comparison of SNR before and after time–frequency filtering across all subjects. Asterisk ∗ indicates a significant difference between SNR of SEP responses before (SNR = 0.046 ± 0.027) and after time–frequency filtering (SNR = 0.14 ± 0.11) (p = 0.001, two tailed Wilcoxon Signed Ranks test).

4.1. Spatial filtering

ICA has been widely applied to decompose a multivariate signal into additive subcomponents under the assumption of mutual statistical independence of the non-Gaussian source signals (Hyvarinen and Oja, 2000; Makeig et al., 1997). When applied to multi-channel EEG recordings (or ERP data), ICA would decompose the signal into the same number of ICs as the total number of recording channels (Makeig et al., 1997; Mouraux and Iannetti, 2008), referred to as unconstrained ICA. However, unconstrained ICA has several critical problems. First, unconstrained ICA is likely to overestimate or underestimate the total number of ICs from multi-channel EEG recordings (Beckmann and Smith, 2004; Mouraux and Iannetti, 2009), which results in either spurious ICs or information loss. Second, unconstrained ICA, especially when applied to EEG recordings from 128 or 256 channels, will dramatically increase the computational complexity (Beckmann, 2004; Beckmann and Smith, 2004). Third, unconstrained ICA is sensitive to errors caused by random noise (Delorme and Makeig, 2004; Tang et al., 2005), and in theory can hardly be used to separate more than one Gaussian distributed sources reliably (Hyvarinen and Oja, 2000).

All these fundamental limitations of unconstrained ICA can be addressed using PICA (Beckmann and Smith, 2004; Mouraux and Iannetti, 2009). First, by constraining the total number of estimated ICs to an effective number of independent sources, PICA is able to provide a more accurate estimation of ICs compared to that of unconstrained ICA. We have shown in this study that the PICA estimated 32 ± 13 ICs from 128-channel EEG recordings, and each obtained IC is more likely to represent a single physiological source of activity (Fig. 2). Second, the problem of high computational complexity when using unconstrained ICA can also be satisfactorily overcome using PICA by constraining the total number of estimated ICs. The PICA can be completed quickly with satisfactory outputs, while unconstrained ICA packages, such as runica routine (Delorme and Makeig, 2004), frequently brought about the "out of memory" message in Matlab (2 CPU of 1.8 GHz and 2 GB RAM)

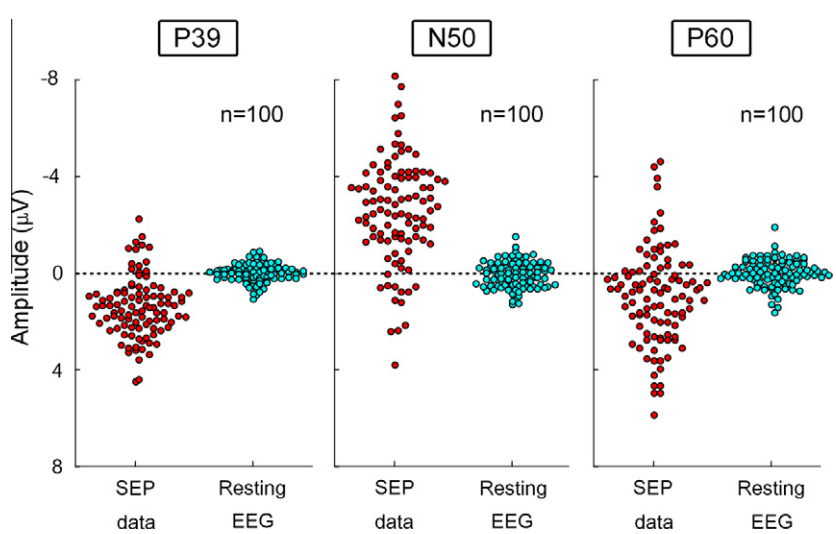

Fig. 6. Comparison of single-trial amplitudes from single-trial SEPs and resting EEG. Each point represents the amplitude of one single trial at their corresponding latencies (number of trials = 100). Amplitudes of SEP trials are often one-side distributed (P39: 1.39 ± 1.23 μV, N50: −2.56 ± 2.17 μV, P60: 0.95 ± 1.96 μV). In contrast, amplitudes of resting EEG trials at the same latencies are distributed around zero (P39: −0.045 ± 0.37 μV, N50: 0.025 ± 0.54 μV, P60: −0.026 ± 0.55 μV). Note that the amplitude values of resting EEG trials were not significantly different from zero (F = 1.429, p = 0.221, one-way ANOVA).

when used for 128-channel EEG recordings. After downsampling the single-trial EEG data from 1000 Hz to 500 Hz, we found that the computation time ratio between unconstrained ICA and PICA was 26 ± 32 times, which verified that PICA is much faster than the unconstrained ICA. Third, using the Gaussian mixture model (Eq. 1), PICA is robust to the random noise contribution in multi-channel EEG recordings (Beckmann, 2004; Beckmann and Smith, 2004). In PICA, the Gaussian noise can be removed by PPCA, before IC estimation, thus resulting in a more accurate IC decomposition compared to the unconstrained ICA.

For these reasons, PICA is adopted in this study instead of the conventional unconstrained ICA as a spatial filter to identify and isolate SEP-related ICs from multi-channel SEP recordings, thus enhancing the SNR of SEP responses, especially in the case of all recorded channels. However, the SNR after PICA is still relatively low, especially in single trials (Fig. 3, middle panel), which may be caused by the large-scale frequency contribution (part of the contribution in some frequency may be caused by noise that is not related to the presentation of sensory stimulus) of the single-trial waveforms. For this reason, time–frequency filtering, which is able to capture the unique time–frequency characteristic of SEPs, is needed.

4.2. Time–frequency filtering

To enhance the SNR of single-trial SEPs to a higher degree, time–frequency filtering, based on CWT, was applied to single-trial SEP responses, which have been preliminary spatial filtered using PICA (Figs. 1 and 3). The CWT can offer an optimal compromise between time and frequency resolution by adjusting the window width as a function of the estimated frequency. Compared with the fixed windowed Fourier transform, the CWT is more suitable for exploring event-related modulations of the EEG spectrum in a wide range of frequencies (Mouraux and Iannetti, 2008), and therefore would provide a more effective time–frequency filter (Effern et al., 2000a,b; Mouraux and Plaghki, 2004; Nenadic and Burdick, 2005; Quiroga and Garcia, 2003; Wang et al., 2007).

The time–frequency filter model was generated by thresholding the time–frequency representation of single trials from all subjects in order to achieve the highest SNR (Fig. 5). Note that 90% of the largest information on the time–frequency plane has been preserved since the time–frequency pixels in the time–frequency filter model were set to 1 when the power of the corresponding wavelet coefficient was larger than 90% of the maximum values. Importantly, the percentage of preserved information on the time–frequency plane can be adjusted by users according to their applications, and thresholds ranging between 80% and 90% would provide very similar results in this study.

4.3. Advantages and potential applications

Single-trial SEP responses with high SNR can be detected from multi-channel EEG recordings by combining PICA-based spatial filtering and CWT-based time–frequency filtering which have several advantages as follows.

First, multi-channel SEP recordings can be decomposed into a limited number of ICs, and SEP-related ICs (Fig. 2) can be identified and separated automatically using the proposed criteria. The pattern of SEP-related ICs (i.e., the waveform shape, scalp topographies and location of dipole sources), which may be influenced by the physiological or pathological changes (e.g., SEP abnormality in comatose patients, and cortical myoclonus patients (Cruccu et al., 2008)), can be effectively detected using PICA for further diagnosis. For this reason, accurate estimation of SEP-related ICs from multi-channel EEG recordings would provide more important information for both basic and clinical applications.

Second, the SNR of SEP recordings, both in average and single trials, can be remarkably enhanced by the space–time–frequency filtering. Considering that the amplitudes of short-latency SEP responses are small (on the order of μV, see Figs. 2, 3, 5 and 6) in relation to the background ongoing EEG (on the order of tens of μV, Fig. 3) in which they are embedded (Rugg and Coles, 1995), the SNR of short-latency SEPs is very low. However, the space–time–frequency filtering provided a good filter performance on the single-trial short-latency SEPs. For this reason, the proposed method is a potentially powerful approach to detect various types of ERPs (both short-latency and long-latency ERPs). Across-trial variability of single-trial ERPs, which may reflect very important physiological or pathological changes, can be detected using the proposed method (Fig. 6). By correlating the single-trial SEP parameters with stimulus parameters (e.g., stimulus intensity, duration, and location) and/or behavioural variables (e.g., the intensity of perception and the reaction time), we are able to investigate and understand new mechanisms of brain processing (Iannetti et al., 2005; Mouraux and Iannetti, 2008). In addition, simultaneous recording of EEG during fMRI will lead to particularly low SNR of EEG data due to the substantial artifacts in the fMRI environment (Mayhew et al., 2006, 2007, 2010; Mouraux and Iannetti, 2008). The proposed method would be useful to detect single-trial ERPs that were simultaneously recorded with fMRI, and investigate the correlation between across-trial variability of ERPs with fMRI responses at single-trial level to study the functional significance of different brain mechanisms (Goldman et al., 2009; Iannetti and Mouraux, 2009; Mayhew et al., 2010; Mobascher et al., 2009; Mouraux and Iannetti, 2008).

Third, by calculating the unmixing matrix $\mathbf{W}_p$, the orthogonalizing matrix $\mathbf{W}_i$ from PICA and the time–frequency model $\mathbf{W}_f$ from the time–frequency filtering (Fig. 1) using training dataset for each subject in advance, the proposed method can be carried out computationally very efficiently. For this reason, this method is promising for applications to real-time SEP extraction, and potentially useful for intraoperative monitoring during surgery to prevent possible and/or potential neurological damage or induced physiological changes (Cruccu et al., 2008; Deletis and Shils, 2002; Hu et al., 2002; Luk et al., 1999, 2001; Nuwer, 1998).

Acknowledgements

L.H. is supported by the Lee Wing Tat Medical Research Fund. Z.G.Z. is partially supported by the HKU CRCG Small Project Funding. Y.H. is partially supported by research grants from the Research Grants Council of the Hong Kong SAR, China (GRF HKU 7130/06E, and GRF 712408E) and from Hong Kong ITF Tier 3(ITS/149/08). All authors have no conflict of interest.

References

Bai X, He B. On the estimation of the number of dipole sources in EEG source localization. Clin Neurophysiol 2005;116:2037–43.
Bai X, He B. Estimation of number of independent brain electric sources from the scalp EEGs. IEEE Trans Biomed Eng 2006;53:1883–92.
Baumgartner U, Vogel H, Ellrich J, Gawehn J, Stoeter P, Treede RD. Brain electrical source analysis of primary cortical components of the tibial nerve somatosensory evoked potential using regional sources. Electroencephalogr Clin Neurophysiol 1998;108:588–99.
Beckmann CF. Probabilistic ICA for FMRI. 2004 2nd IEEE international symposium on biomedical imaging: macro to nano, vol. 1 and 2. 2004. p. 1490–93.
Beckmann CF, Smith SM. Probabilistic independent component analysis for functional magnetic resonance imaging. IEEE Trans Med Imaging 2004;23:137–52.
Bell AJ, Sejnowski TJ. An information-maximization approach to blind separation and blind deconvolution. Neural Comput 1995;7:1129–59.
Bingham E, Hyvarinen A. A fast fixed-point algorithm for independent component analysis of complex valued signals. Int J Neural Syst 2000;10:1–8.
Blum AS, Rutkove SB. The clinical neurophysiology primer. Totowa, NJ: Humana Press; 2007.

Britton J, Jervis BW, Grunewald RA. Extracting single trial event related potentials. IEEE Proc – Sci, Meas Technol 2000;147:382–8.
Cruccu G, Aminoff MJ, Curio G, Guerit JM, Kakigi R, Mauguiere F, Rossini PM, Treede RD, Garcia-Larrea L. Recommendations for the clinical use of somatosensory-evoked potentials. Clin Neurophysiol 2008;119:1705–19.
Dawson GD. A summation technique for detecting small signals in a large irregular background. J Physiol 1951;115:2p–3p.
Dawson GD. A summation technique for the detection of small evoked potentials. Electroencephalogr Clin Neurophysiol 1954;6:65–84.
Debener S, Strobel A, Sorger B, Peters J, Kranczioch C, Engel AK, Goebel R. Improved quality of auditory event-related potentials recorded simultaneously with 3-T fMRI: removal of the ballistocardiogram artefact. Neuroimage 2007;34:587–97.
Deletis V, Shils JL. Neurophysiology in neurosurgery: a modern intraoperative approach. San Diego, CA: Academic Press; 2002.
Delorme A, Makeig S. EEGLAB: an open source toolbox for analysis of single-trial EEG dynamics including independent component analysis. J Neurosci Methods 2004;134:9–21.
Effern A, Lehnertz K, Fernandez G, Grunwald T, David P, Elger CE. Single trial analysis of event related potentials: non-linear de-noising with wavelets. Clin Neurophysiol 2000a;111:2255–63.
Effern A, Lehnertz K, Grunwald T, Fernandez G, David P, Elger CE. Time adaptive denoising of single trial event-related potentials in the wavelet domain. Psychophysiology 2000b;37:859–65.
Goldman RI, Wei CY, Philiastides MG, Gerson AD, Friedman D, Brown TR, Sajda P. Single-trial discrimination for integrating simultaneous EEG and fMRI: identifying cortical areas contributing to trial-to-trial variability in the auditory oddball task. Neuroimage 2009;47:136–47.
Hu Y, Luk KD, Lu WW, Holmes A, Leong JC. Comparison of time–frequency distribution techniques for analysis of spinal somatosensory evoked potential. Med Biol Eng Comput 2001a;39:375–80.
Hu Y, Luk KD, Wong YW, Lu WW, Leong JC. Effect of stimulation parameters on intraoperative spinal cord evoked potential monitoring. J Spinal Disord 2001b;14:449–52.
Hu Y, Luk KD, Lu WW, Leong JC. Comparison of time–frequency analysis techniques in intraoperative somatosensory evoked potential (SEP) monitoring. Comput Biol Med 2002;32:13–23.
Hu L, Mouraux A, Hu Y, Iannetti GD. A novel approach for enhancing the signal-to-noise ratio and detecting automatically event-related potentials (ERPs) in single trials. Neuroimage 2010;50:99–111.
Hyvarinen A. Fast and robust fixed-point algorithms for independent component analysis. IEEE Trans Neural Netw 1999;10:626–34.
Hyvarinen A, Oja E. Independent component analysis: algorithms and applications. Neural Netw 2000;13:411–30.
Iannetti GD, Mouraux A. Combining EEG and fMRI in pain research. In: Mulert C, Lemieux L, editors. EEG-fMRI: physiological basis, technique, and applications. London: Springer; 2009. p. 365–84.
Iannetti GD, Zambreanu L, Cruccu G, Tracey I. Operculoinsular cortex encodes pain intensity at the earliest stages of cortical processing as indicated by amplitude of laser-evoked potentials in humans. Neuroscience 2005;131:199–208.
Iannetti GD, Hughes NP, Lee MC, Mouraux A. Determinants of laser-evoked EEG responses: pain perception or stimulus saliency? J Neurophysiol 2008;100:815–28.
Jongsma MLA, Eichele T, Van Rijn CM, Coenen AML, Hugdahl K, Nordby H, Quiroga RQ. Tracking pattern learning with single-trial event-related potentials. Clin Neurophysiol 2006;117:1957–73.
Jung TP, Makeig S, Westerfield M, Townsend J, Courchesne E, Sejnowski TJ. Analysis and visualization of single-trial event-related potentials. Hum Brain Mapp 2001;14:166–85.
Kraft GH, Aminoff MJ, Baran EM, Litchy WJ, Stolov WC. Somatosensory evoked potentials: clinical uses. AAEM Somatosensory Evoked Potentials Subcommittee. American Association of Electrodiagnostic Medicine. Muscle Nerve 1998;21:252–8.
Liang M, Mouraux A, Chan V, Blakemore C, Iannetti GD. Functional characterisation of sensory ERPs using probabilistic ICA: effect of stimulus modality and stimulus location. Clin Neurophysiol 2010;121:577–87.
Luk KD, Hu Y, Wong YW, Leong JC. Variability of somatosensory-evoked potentials in different stages of scoliosis surgery. Spine (Phila Pa 1976) 1999;24:1799–1804.
Luk KD, Hu Y, Lu WW, Wong YW. Effect of stimulus pulse duration on intraoperative somatosensory evoked potential (SEP) monitoring. J Spinal Disord 2001;14:247–51.
Makeig S, Jung TP, Bell AJ, Ghahremani D, Sejnowski TJ. Blind separation of auditory event-related brain responses into independent components. Proc Natl Acad Sci USA 1997;94:10979–84.
Mauguiere F, Allison T, Babiloni C, Buchner H, Eisen AA, Goodin DS, Jones SJ, Kakigi R, Matsuoka S, Nuwer M, Rossini PM, Shibasaki H. Somatosensory evoked potentials. The International Federation of Clinical Neurophysiology. Electroencephalogr Clin Neurophysiol Suppl 1999;52:79–90.
Mayhew SD, Iannetti GD, Woolrich MW, Wise RG. Automated single-trial measurement of amplitude and latency of laser-evoked potentials (LEPs) using multiple linear regression. Clin Neurophysiol 2006;117:1331–44.
Mayhew SD, Dirckx SG, Niazy RKN, Iannetti GD, Wise RG. Auditory-evoked scalp potentials may be recorded simultaneously with continuous fMRI scanning. 13th Annual meeting human brain mapping, Chicago; 2007.
Mayhew SD, Dirckx SG, Niazy RK, Iannetti GD, Wise RG. EEG signatures of auditory activity correlate with simultaneously recorded fMRI responses in humans. Neuroimage 2010;49:849–64.
Minahan RE. Intraoperative neuromonitoring. Neurologist 2002;8:209–26.
Minka TP. Automatic choice of dimensionality for PCA. Adv Neural Inform Process Syst 2001;13(13):598–604.
Mobascher A, Brinkmeyer J, Warbrick T, Musso F, Wittsack HJ, Saleh A, Schnitzler A, Winterer G. Laser-evoked potential P2 single-trial amplitudes covary with the fMRI BOLD response in the medial pain system and interconnected subcortical structures. Neuroimage 2009;45:917–26.
Mouraux A, Iannetti GD. Across-trial averaging of event-related EEG responses and beyond. Magn Reson Imaging 2008;26:1041–54.
Mouraux A, Iannetti GD. Nociceptive laser-evoked brain potentials do not reflect nociceptive-specific neural activity. J Neurophysiol 2009;101:3258–69.
Mouraux A, Plaghki L. Single-trial detection of human brain responses evoked by laser activation of Adelta-nociceptors using the wavelet transform of EEG epochs. Neurosci Lett 2004;361:241–4.
Nenadic Z, Burdick JW. Spike detection using the continuous wavelet transform. IEEE Trans Biomed Eng 2005;52:74–87.
Nishida S, Nakamura M, Shibasaki H. Method for single-trial recording of somatosensory evoked potentials. J Biomed Eng 1993;15:257–62.
Nuwer MR. Spinal cord monitoring with somatosensory techniques. J Clin Neurophysiol 1998;15:183–93.
Nuwer MR, Aminoff M, Desmedt J, Eisen AA, Goodin D, Matsuoka S, Mauguiere F, Shibasaki H, Sutherling W, Vibert JF. IFCN recommended standards for short latency somatosensory evoked potentials. Report of an IFCN committee. International Federation of Clinical Neurophysiology. Electroencephalogr Clin Neurophysiol 1994;91:6–11.
Pfurtscheller G, Lopes da Silva FH. Event-related EEG/MEG synchronization and desynchronization: basic principles. Clin Neurophysiol 1999;110:1842–57.
Quiroga RQ. Obtaining single stimulus evoked potentials with wavelet denoising. Phys D-Nonlinear Phenomena 2000;145:278–92.
Quiroga RQ, Garcia H. Single-trial event-related potentials with wavelet denoising. Clin Neurophysiol 2003;114:376–90.
Rossi L, Bianchi AM, Merzagora A, Gaggiani A, Cerutti S, Bracchi F. Single trial somatosensory evoked potential extraction with ARX filtering for a combined spinal cord intraoperative neuromonitoring technique. Biomed Eng Online 2007;6:2.
Roweis S. EM algorithms for PCA and SPCA. Adv Neural Inform Process Syst 1998;10(10):626–32.
Rugg MD, Coles MGH. Electrophysiology of mind: event-related brain potentials and cognition. Oxford, England: Oxford University Press; 1995.
Schwarz G. Estimating the dimension of a model. Ann Stat 1978;6:461–4.
Spencer KM. Averaging, detection, and classification of single-trial ERPs. In: Handy TC, editor. Event-related potentials: a methods handbook. Cambridge, Mass.: MIT Press; 2005. p. 209–27.
Tang AC, Sutherland MT, McKinney CJ. Validation of SOBI components from high-density EEG. Neuroimage 2005;25:539–53.
Tipping ME, Bishop CM. Mixtures of probabilistic principal component analyzers. Neural Comput 1999a;11:443–82.
Tipping ME, Bishop CM. Probabilistic principal component analysis. J R Stat Soc Ser B 1999b;61:611–22.
Tognola G, Grandori F, Ravazzani P. Wavelet analysis of click-evoked otoacoustic emissions. IEEE Trans Biomed Eng 1998;45:686–97.
van de Wassenberg W, van der Hoeven J, Leenders K, Maurits N. Multichannel recording of median nerve somatosensory evoked potentials. Neurophysiol Clin 2008a;38:9–21.
van de Wassenberg WJ, Kruizinga WJ, van der Hoeven JH, Leenders KL, Maurits NM. Multichannel recording of tibial-nerve somatosensory evoked potentials. Neurophysiol Clin 2008b;38:277–88.
Wang ZS, Maier A, Leopold DA, Logothetis NK, Liang HL. Single-trial evoked potential estimation using wavelets. Comput Biol Med 2007;37:463–73.
Wiedemayer H, Fauser B, Sandalcioglu IE, Schafer H, Stolke D. The impact of neurophysiological intraoperative monitoring on surgical decisions: a critical analysis of 423 cases. J Neurosurg 2002;96:255–62.